JOURNAL LA MULTIAPP

VOL. 03, ISSUE 04 (131-154), 2022
DOI: 10.37899/journallamultiapp.v3i4.674

Development of Wind Turbine Generator and Solar Hybrid Power System Model for Rural Electrification

Ola Austin Oshin[1]

[1]*Department of Electrical Electronics Engineering, Elizade University, Ilara-Mokin, Ondo State, Nigeria*

**Corresponding Author: Ola Austin Oshin*
Email: austin.oshin@elizadeuniversity.edu.ng

Article Info

Article history:
Received 24 June 2022
Received in revised form 11 August 2022
Accepted 15 August 2022

Keywords:
Solar
Hybrid Power
Rural Electrification

Abstract

The countries that are most energy-consuming, where there are industrial developments, where the energy demand is highest are the advanced and developing countries in the world (Mustafa, 2018). For instance, the average power per capital (watts per person) in the United States is 1,377 Watts. In Canada, it is as high as 1,704 Watts per person and in South Africa; it is 445 Watts per person. The average power per capital in Australia is 1,112 Watts and in New Zealand it is 1,020 W per person. Whereas, the average power per capital (watts per person) in Nigeria is 14 W per person. (Austin, O. O et.al, 2020). Also, power supply in many parts of Africa is erratic and characterized with a lot of faults and outages. In Nigeria, it is estimated that only 40 % of Nigerians are connected to the national grid and the connected population are exposed to frequent power outages (Abubakar et al, 2015, Austin O.A, 2020). Unfortunately, the effects of incessant power supply have destroyed many industrial activities, reduced employment and has increased crime activities in many parts of the continent (Africa). Therefore, in order to provide urgent solution to these problems and satisfy the high energy demand in African residential and industrial environments, electrical energy should be reliable, affordable, effective, and sustainable. This calls for an urgent establishment of alternative Renewable Hybrid Power Supply System which will provide continuous, reliable and effective power supply to the consumers.

Introduction

Hence, in this research work, feasibility assessment of the study area for the establishment of Hybrid Power System (HPS) was carried out. The operating parameters and performances of the components of the Hybrid Power System were evaluated and the HPS Simulink models were developed using MATLAB/Simulink 8.1064 (2020a) version software. The Hybrid Power System Model (HPSM) developed comprises of Solar Photo Voltaic System (SPVS) and Wind Turbine Generator (WTG) Models. Simulation of the developed Simulink models were carried out. Optimization process was carried out using Optimum Power Point Tracking (OPPT)Techniques and Genetic Algorithms (G.A). Design processes and control algorithms were established for the production of reliable and efficient output power from the Hybrid Power System. Simulink and validation results obtained made it possible to generate and supply continuous, reliable, effective and stable electrical power to the consumers. Finally, the developed HPS model in this research work was found to be very useful for the establishment of Hybrid Power Plants which guarantees the supply of continuous, stable and reliable electric power for various residential and industrial consumers.

Aim of the Research

The aim of the research is to develop a wind and solar Hybrid Power System Model for the operation and design of renewable energy system and develop an effective Hybrid Power System model with Optimum Performance using Optimum Power Point Tracking (OPPT) Techniques.

Objectives of the Research Work

(1) To evaluate the operating parameters and performances of the components of the Hybrid Power System Model (HPSM); (2) To develop Simulink models of the HPSM using MATLAB/Simulink 8.1.0604 (2020a) version software; (3) To develop an effective Hybrid Power System model with Optimum Performance using Optimum Power Point Tracking (OPPT) Techniques.

Introduction to Hybrid Renewable Energy System

Current nonrenewable energy sources are insufficient to supply the ever-increasing demand for electricity. Consequently, there is an urgent need to use the energy that may be obtained from renewable sources. Emerging alternatives, such as hybrid renewable energy sources, provide a solution to both the endless supply of power provided by nonrenewable energy sources and the insufficient quantity of energy supplied by such sources. It is the integration of two or more renewable energy sources that may operate independently or in tandem with an existing power grid. Alternately, it may refer to the combination of two or more renewable energy sources, with or without conventional energy sources. Hybrid renewable energy systems, commonly referred to as hybrid electric power systems, use both traditional and alternative kinds of renewable energy sources (HEPS). A hybrid energy system combines two or more unique kinds of energy sources to obtain the best degree of performance achievable. This reduces the negative impacts associated with each unique energy source (Kyari, et. al, 2019).

Literature Review

Operating Performances of the Solar Photovoltaic System (SPVS)

As illustrated in figure 2.1, a photovoltaic module or array is constructed up of a number of solar cells that are linked in series and parallel with one another. There are no moving elements involved in the conversion of light energy to electrical energy that takes place when solar light radiation strikes PV cells. Within the semiconductor, the light that is transmitted is absorbed, and electrical energy is produced by using the light energy to excite free electrons from their low energy state to an unoccupied higher energy level. This process is called photoexcitation. As a direct consequence of this, combinations of electrons and holes will take place at the p-n junction of the semiconductor diode, which will ultimately lead to the passage of electrical current. The solar photovoltaic module's IV and PV properties will change depending on the temperature and irradiance circumstances that are present.

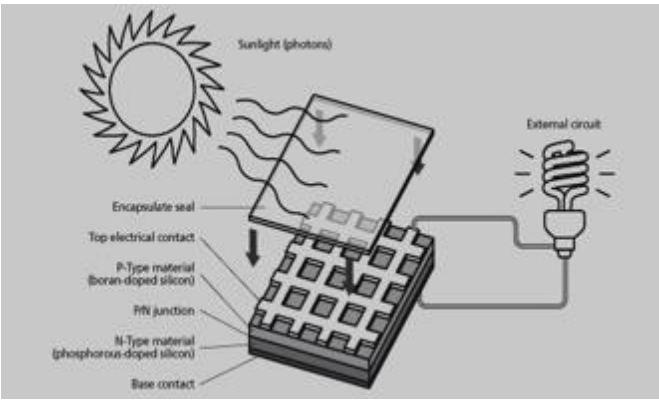

Figure 1. Conversion of light energy to electrical energy in a Solar PV module

Single Diode Model with Shunt Resistance

The solar PV circuit model shown in figure 2.2 contains the current source I_{ph} which depends on cell temperature and solar radiation, a diode in which the reverse saturation current (I_D) depends mainly on the operating temperature, a series resistance (R_s). and a shunt resistance (R_{sh} or R_p) which takes into account the losses in PV cell (Jain & Ramteke, 2013).

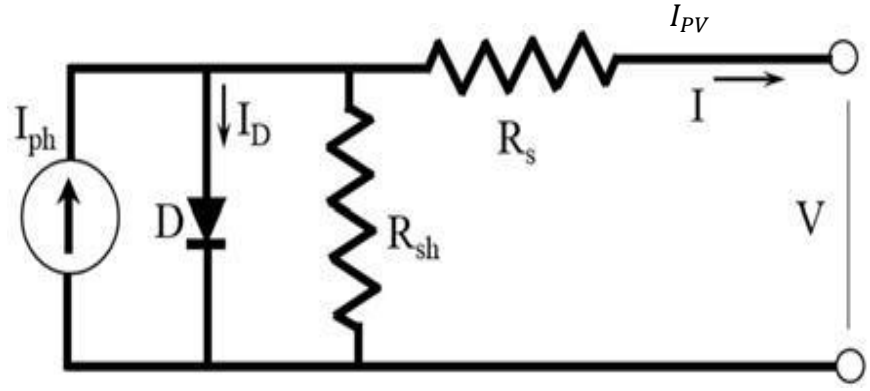

Figure 2. A Single Diode Model with Shunt Resistance

Model equations of the output current of the solar photovoltaic is presented in equations 2.1 – 2.4.

$$I_{PV} = N_P I_{ph} - N_P I_S \left[. \exp \frac{\left(\frac{V}{N_S} + \frac{I R_S}{N_p}\right)}{AKT} - 1 \right] - \left[\frac{\frac{V * N_P}{N_S} + IR_S}{R_{sh}} \right] \text{…….. 2.1}$$

Where:

i. N_P = number of parallel cells

ii. N_s = number of series cells

iii. $I_{PV} = output\ current$, I_D = Diode current

iv. $I_{ph=}$ light generated photo current

v. $I_{rs\ =}$cell reverse saturation current at T_{ref}

vi. I_{SC} = Short circuit current at reference temperature 25º C

vii. I_S = Cell saturation current current at T_{ref}

viii. $T_{nom} = T_{ref}$ = reference temperature in celsius

ix. The reference values will be taken from the PV module manufacturers datasheet for specified operating condition such as STC (standard test conditions) in which the irradiance is 1000W/m^2

x. K_i = Short circuit current temperature coefficient at I_{SCR}

xi. K = Boltzmann's constant 1.38 * 10^{-23} J/K

xii. T = Cell temperature in Celsius

xiii. q = Charge of electron = 1.6 x 10^{-19} C

xiv. λ = Solar irradiation in Watts/m^2

xv E_g= Band gap energy for silicon and A = Ideality factor

xvi. T_{nom}= T_{ref} = Reference temperature in Celsius = 25 degree celsius

$xvii$. I_S = Cell saturation current at T_{nom}

$xviii$. R_{sh} = Shunt resistance in ohms

xix. R_s = Series resistance in oh

The reverse saturation current (Irs) gis given in equation 2.2

$$I_{rs} = I_{SC} / \left[. \exp \frac{(q * V_{oc})}{N_s AKT} - 1 \right] \quad 2.2$$

When a diode is exposed to a reverse bias, the depletion region widens and the bulk of carriers move away from the junction. Consequently, the majority carriers no longer contribute to the current flow. There are, however, forward-biased minority electron-hole pair pairings that are thermally produced while the actual bias is reverse. These minority carriers must be present in order for current to flow across the circuit. This current is often rather insignificant (within the range of micro amp to nano amp). This current is known as a reverse saturation current because its flow is produced by minority carriers at a certain temperature.

Reverse-saturation current in a semi-conductor diode depends strongly on temperature. This is because, minority carriers are thermally generated in p-n junction diode. Hence, reverse saturation current is not affected by the reverse bias but highly affected by temperature changes. The saturation current (Is) is given in equation 2.3

$$I_S = I_{rs} \left[\frac{T}{T_r}\right]^3 \left[\exp \left(E_{g*} \frac{q\,(T - T_r)}{A*\ K.T.T_r} \right) \right] \quad 2.3$$

Observation revealed that the photocurrent I_{ph} varies with cell short circuit current I_{SCR} , cell temperature T, cell referred temperatureT_r, short circuit current temperature coefficient k_1 and solar radiation S (in mW/cm^3) as shown in the equation 2.4:

$$I_{ph} = \left[I_{SCR} + k_1 [T - T_r]\right] \frac{S}{100} \quad 2.4$$

The Practical Single Diode PV Cell Model

Figure 3 shows a practical single PV cell model with the mathematical model equations shown in equations 2.5 – 2.7

$$I = I_{ph} - I_D - I_{sh} \quad 2.5$$

I = cell current, $I_{ph} = photo\ current$, I_D = diode current, A = diode constant, q = charge of the electron, K = Boltzmaan's constant, I_0 = cell saturation current, V = cell voltage

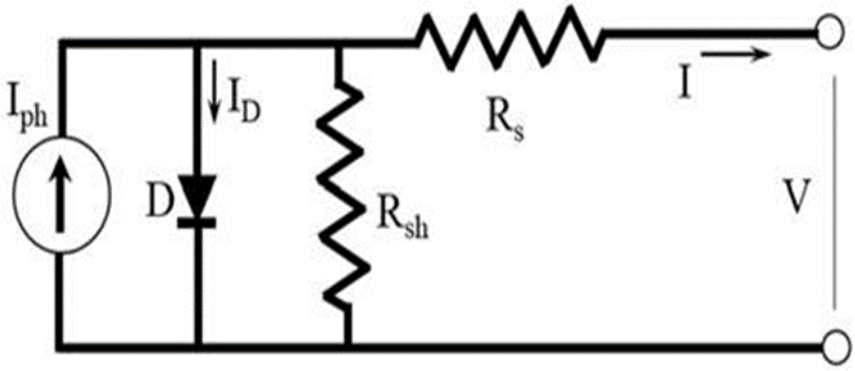

Figure 3. Practical Single PV Cell Model

T = cell temperature (K), R_s = series resistance and $R_{sh} = shunt\ resistance$

Diode current $I_D = I_0 \left[. \exp\left(\frac{q\,(V + I\,R_s)}{AKT} - 1 \right) - \frac{(V + I\,R_s)}{R_{sh}} \right]$ 2.6

Therefore, I = $I_{ph} - I_D$ *will become*

$$I = I_{ph} - I_0 \left[. \exp\left(\frac{q\,(V + I\,R_s)}{AKT} - 1 \right) - \frac{(V + I\,R_s)}{R_{sh}} \right] \quad 2.7$$

Maximum Power Point Techniques (Mppt) in A Wtg Using Tip Speed Ratio (Tsr) Control Techniques

Tip Speed Ratio (TSR) control techniques may be used to modify the amount of electricity generated by the generator of a wind turbine. In order to reach this objective, the variable speed generator's Tip Speed Ratio must be maintained at its optimal value. Consequently, the objective of this Maximum Power Point Techniques (MPPT) approach is to determine the best TSR by calculating it based on the recorded wind speed and rotor speed using the mathematical model equation presented further down in this paragraph.

The Tip Speed Ratio = $\frac{R\omega}{V}$

Where R = Radius of the turbine (m)

ω = angular speed of the tip of a blade in rad/sec

V = average wind speed in m/s

The optimum tip speed ratio λ_{opt} is attained when the coefficient of performance C_p of the WTG is maximum as shown in the figure 2.4. For Wind Turbine generator, coefficient of performance C_p is less or equal to 0.593

The maximum rotor speed of the wind Turbine generator can then be obtained

Optimum rotor speed = $\omega_{optimum} = \frac{\lambda_{optimum}}{R}\ V_{windspeed}$ 2.8

Hence, the maximum Power Point is obtained when the rotor is running at optimum rotor speed ($\omega_{optimum}$). Maximum Power Point is obtained when the turbine shaft (ω_r) is optimum as shown in figure 4.

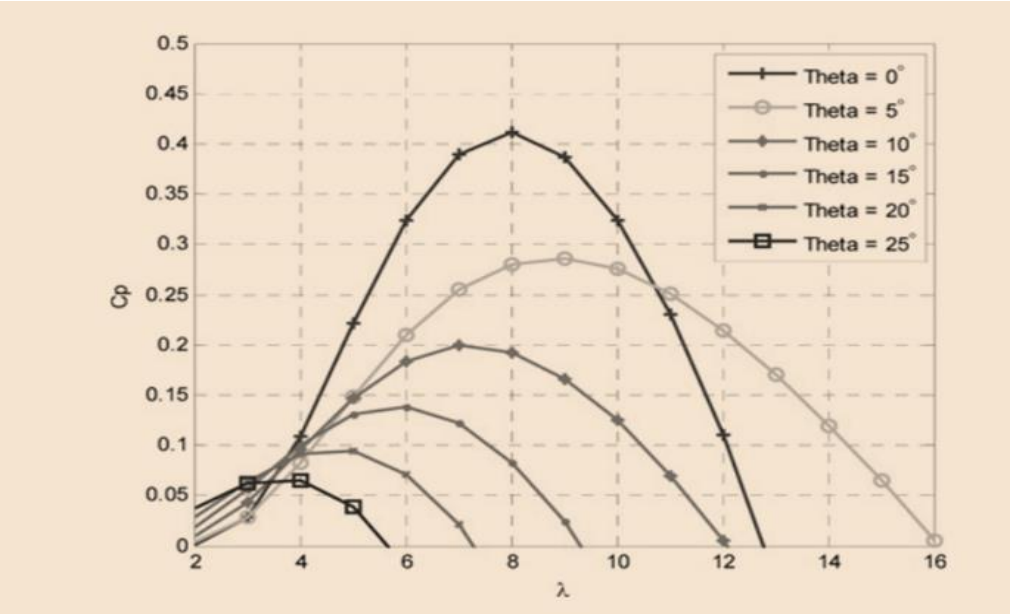

Figure 4. Showing the Coefficient of Performance, C_p, and the Tip Speed Ratio λ

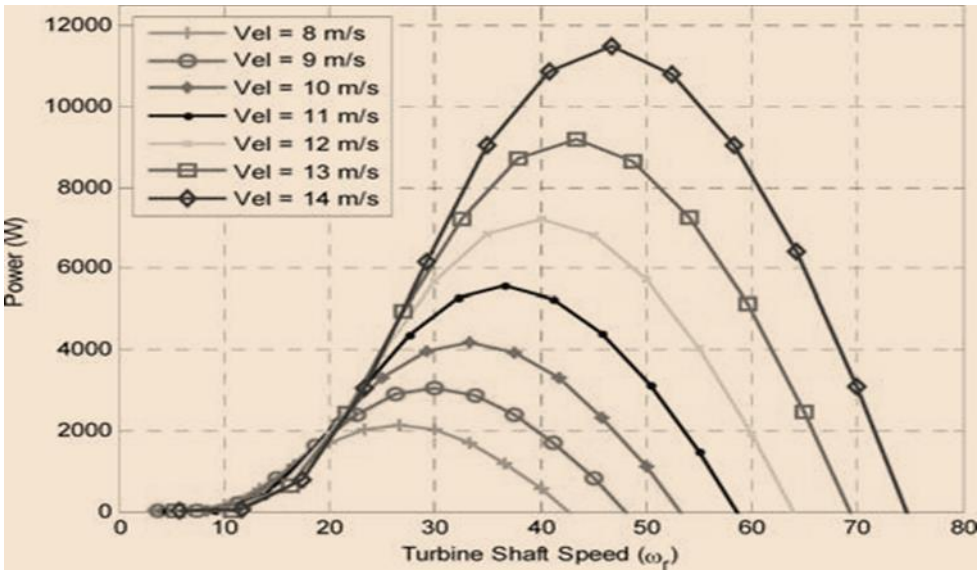

Figure 5. Wind Turbine Power Curve

If the angular speed is larger than the reference or planned turbine shaft speed at which maximum power may be produced, the angular speed must be lowered to get optimum output power. This will let the turbine to generate its maximum output power. If the angular speed is lower than the turbine shaft speed at which maximum power may be generated, the angular speed should be increased. Highest Power Point Tracking is the process of adjusting the turbine's angular speed in order to provide the maximum output power. This method is known as Maximum Power Point.

Maximum Power Point Tracking Techniques

In contrast to diesel power plants and generators, solar and wind energy require a control system that is one-of-a-kind. Diesel power plants and generators are able to modulate the speed of the rotor, change the magnetic field around the stator and rotor, and control the amount of fuel that flows through the system. It is possible to reach the Maximum Power Point in a Wind Turbine Generator (WTG) by using the Hill Climb Searching (HCS) or Perturb and Observe (P & O) iteration strategy, as well as Optimum Torque Control (OTC) and Optimum Tip Speed Ratio Control (OTSR). The amount of electrical energy that may be generated by the generator

of a wind turbine is directly proportional to the rotor's rotational speed. Changes need to be made to the rotational speed in order to realize the ideal Tip Speed Ratio (TSR) shown in figures 2.4 and 2.5.

The Tip Speed Ratio was determined by dividing the spinning speed of a blade's tip by the wind speed, V, in a particular direction. This calculation was performed for each blade. It was determined with the help of a tachometer how fast the blade was moving. An anemometer was used in order to get a reading on the wind speed. The TSR value that was calculated as a consequence was evaluated in light of the ideal TSR value that had been entered into the generator. This was done on a continuous basis, and the difference was sent back to the controller. The controller then altered the speed of the WTG so that it could function at or near the ideal value of the TSR. Maintaining optimal TSR enables a Wind Turbine Generator to generate electricity at maximum output and efficiency.

Maximum Power Point Tracking Techniques in Solar Photo-Voltaic System

In a photo-voltaic System, maximum power point can be obtained by varying solar insolation. This can be done by using stepper motor control system, Perturb and Observe (P & O) or Hill Climb Searching (HCS) iteration method, Open Circuit Based MPPT Techniques (OCBT), Incremental Conductance Method (ICM), Look Up Table and Curve Fitting Method (LTCFM), and Parasitic Capacitance Algorithm (PCA). With these MPPT tracking techniques, installation cost will reduce, efficiency will increase, the performance and efficiency of the hybrid system will increase.

Perturb and Observe Method (P & O)

Due to the simplicity of its feedback structure and the minimal number of evaluable parameters, P&O is the method that is most often and widely applied. P&O for a solar system comprises adjusting the solar output voltage by increasing or reducing it on a regular basis and observing the effect on the system's power output. If a specific perturbation increases the array's power, further perturbations are done in the same direction. In the event that this is not the case, following perturbations are executed in the other direction. When the derivative of the fluctuating output power to voltage shown in Figure 2.6 is zero, the maximum output power is obtained. This can be seen in the picture.

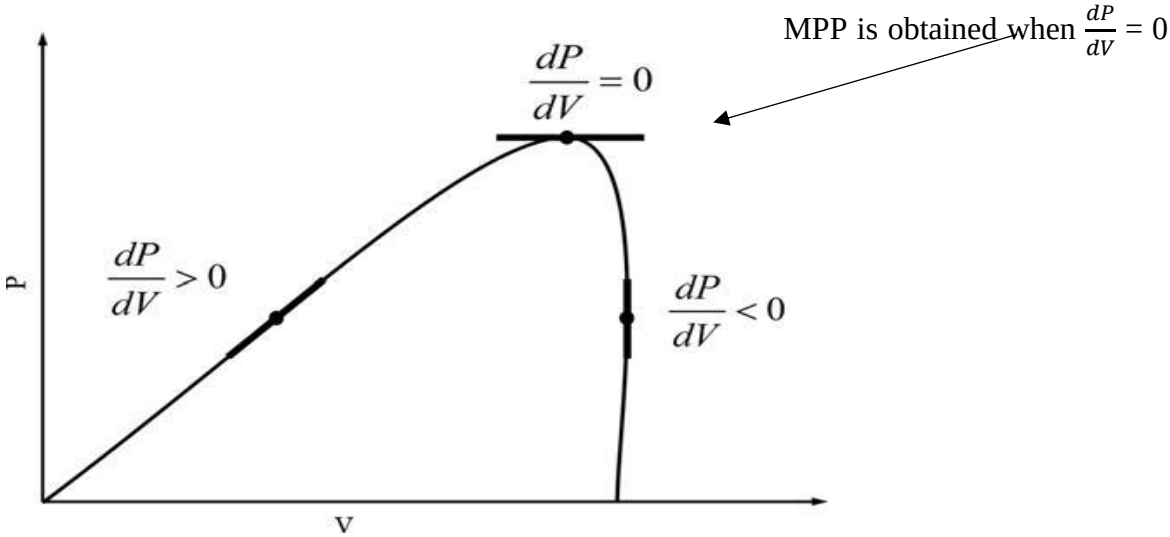

Figure 6. Maximum Power Point Tracking in Solar Photo-Voltaic System

Modelled Wind Power System

The model equation for wind power system is shown in equation 2.9:

$$P_{wind} = \frac{1}{2}\ C_p\ \lambda\rho\ A\ \ V^3 \qquad 2.9$$

Where

(P) = Power Output of the wind turbine in kilowatts

(ρ) = Air Density, measured in kilogram per cubic meter

(A) = intercepting area of the rotor blade in square meter

(V) = Wind Speed, miles/seconds

λ = Tip Speed Ratio (TSR)

(Cp) = Turbine power efficiency coefficient or coefficient of performance, Bertz coefficient which is a maximum of 0.593.

Methods

This research work developed a Hybrid Power System Model for feasibility assessment and establishment of renewable energy. It provides reliable, efficient and low-cost electric power from Hybrid Electric Power System (HEPS) model shown in figure 3.1.

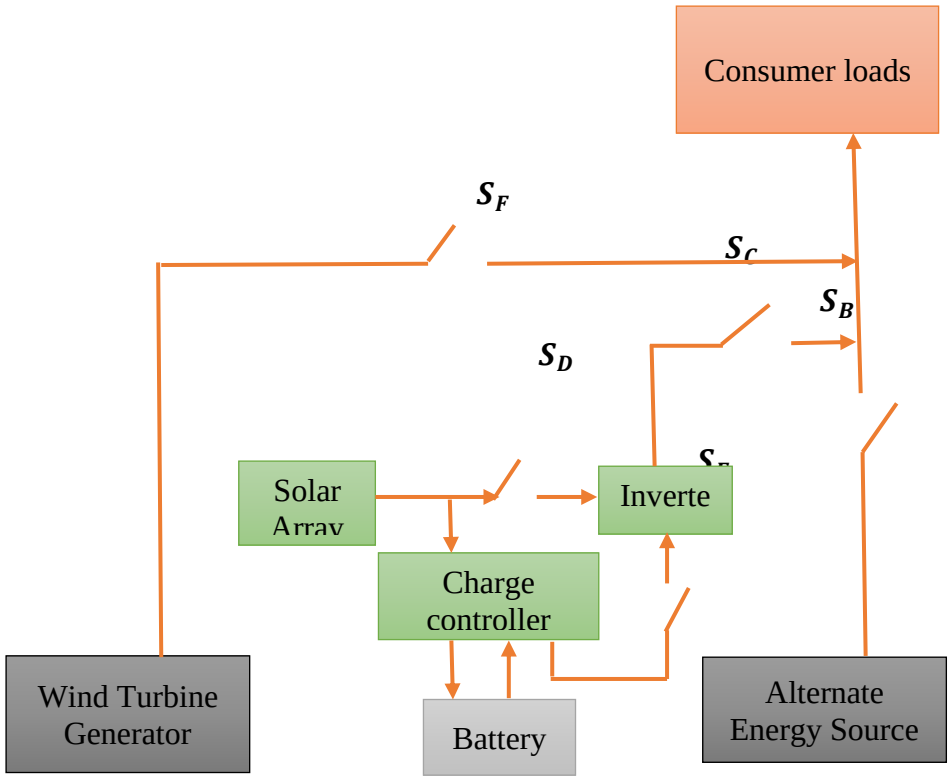

Figure 7. Hybrid Electric Power System (HEPS)

Energy Consumption and Meteorological Data Analysis

Energy audit data and Meteorological data were collected from Kwara State University with energy consumption in watt hour given as 1,865,500 Watt hour

This implies that the total energy to be supplied = 1,865,500 Wh

Watt peak = $\frac{\text{Energy to be supplied}}{number\ of\ hours\ of\ sunlight} = \frac{1{,}865{,}500\ \text{Wh}}{7} = 266{,}500$

Number of 325 W panels = $\frac{\text{Watt peak}}{Wattage\ of\ a\ solar\ panel} = \frac{266{,}500}{325} = 820$

System voltage = Voltage of a battery x number of batteries in series = 12 X 82 = 924 V

Charge to be stored in the solar system = $\frac{Grand\ total\ energy\ x\ Day(s)\ of\ autonomy}{nomoinal\ Voltage}$ 3.1

Charge to be stored in the solar system = $\frac{1{,}865{,}500\ x\ 1}{12}$ = 155,485.33 Ampere hour (Ah)

System Current = $\frac{\text{Total power}}{system\ voltage}$ = $\frac{245{,}073.4}{924}$ = 265.231 A

Land Area = Area of one module x number of modules = 1.63 x 820 = 1,328.4m^2

200 Ah batteries were used at the reference area

Hence, number of batteries required = $\frac{\text{Charge to be stored in the solar system}}{0.85\ x\ rating\ of\ a\ battery\ in\ Ah\ x\ depth\ of\ discharge}$ 3.2

The depth of discharge is 70% while 0.85 accounts for battery loss

Hence, number of batteries required = $\frac{155{,}485.33}{0.85\ x\ 200\ x\ 0.7}$ = 1306.599, approximately equal to 1,307

Latitude (ψ) and longitude of the location are $8^0\ N$, 5^0 E respectively

Average solar insolation: 278–330 days of sun per year with daily average sunshine ranging from 6 hours during the rainy season to 9 hours in dry season

Solar radiation is the incident energy per unit area on a surface. Solar irradiance (SI) is the power per unit area (watt per square metre, W/m^2) received from the Sun in the form of electromagnetic radiation Maximum power is generated when the tilt angle is equal to the latitude of the location.

The monthly average clear sky daily global irradiance (H_C) for the location in Wh/m^2 /day can be estimated using equation 3.9.

$$H_C = \frac{24\ X\ I_{sc}}{\pi}\left[1 + 0.033\cos\left(\frac{360n}{365}\right)\right]\text{xcos ø cos δ sin } w_s + \left(\frac{2\pi w_s}{360}\right)\text{sin ø sin δ} \quad 3.3$$

I_{sc} = solar constant = 1000 W/m^2

n = average daylight length

N = maximum possible sunshine duration

H = monthly average daily global radiation in Wh/m^2/day

H_C = monthly average clear sky daily global radiation for the location in Wh/m^2 /day

a and b are empirical constants

E_o = eccentricity correction = $1 + 0.033\cos\left(\frac{360nd}{365}\right)$

Where nd is the number of days in the year starting 1st of January to December 31st = 365, E_o = eccentricity correction = $1 + 0.033\cos\left(\frac{360nd}{365}\right)$ 3.4

$= 1 + 0.033\cos 360 = 1.33$

The angle measured from the centre of the sun to the centre of the earth is known as angle of declination δ. This value for the study area was obtained using equation 3.5

$$\delta = 23.45\sin\left[360\ \left(\frac{284 + n}{365}\right)\right] \quad 3.5$$

$= 23.45\sin\left[360\ \left(\frac{284 + 365}{365}\right)\right] = 23.45\sin\left[360\ \left(\frac{649}{365}\right)\right]$

$= 23.45\sin[640.11] = 23.086$

Latitude of the location = ψ = $8^0\ 24' = 8.4^0$, daily average value of sun shine length N = $\frac{2}{15}W_s$

Where W_s = mean sunset hour angle, N = daily average value of sun shine length and n = number of hours in a day

$$a = -0.11 + 0.235 \cos \psi + 0.323 \frac{n}{N} \quad (3.6)$$

$$= -0.11 + 0.235 \cos 8.4 + 0.323 \frac{24}{7} = -0.11 + 0.2323 + 1.1074 = 1.2297$$

$$b = 1.45 + 0.553 - 0.694 \frac{n}{N} \quad (3.7)$$

$$= 1.45 + 0.553 - 0.694 \frac{24}{7} = -0.3764$$

Where, clearness index, $K_t = \frac{H}{H_o} = a + b\left[\frac{n}{N}\right]$ (3.8)

$$\frac{H}{H_o} = 1.2297 + -0.3764\left[\frac{24}{7}\right] = -0.0606$$

The clearness index quantifies the atmosphere's transparency. It is calculated by dividing the surface radiation by the extraterrestrial radiation. It is the proportion of solar energy that is passed through the atmosphere to reach the earth's surface.

Results and Discussion

Results of the Output Current of the Photovoltaic Cell

The output current of the Photovoltaic cell, I, under varying irradiance and temperature were obtained using equations 4.1 – 4.3 and the results were simulated using Matlab Simulink Software.

$$I = I_{ph} - I_s\left[\exp\left(\frac{qV_{oc}}{AkT_c}\right) - 1\right] \quad (4.1)$$

$$I_{ph} = \left[I_{sc} + K_i\left(T_C - T_{ref}\right)\right] \quad (4.2)$$

$$I_S = I_{RS}\left[\frac{T_c}{T_{ref}}\right]^3 \exp\left[\frac{q\,E_G\left(\frac{1}{T_{ref}} - \frac{1}{T_c}\right)}{KA}\right] \quad (4.3)$$

I = output current of the Photovoltaic cell

I_{ph} = photo current

I_s = saturation current

q= elementary charge = (1.6022×10^{-19}) C

V_{oc} = open circuit voltage of a module = 3.1 V

A = Ideality factor (IF) = 1.13

K=Boltzmann's constant = $1.38\ x\ 10^{-23}$ J/K

T_c = temperature of the location

I_{sc} = short circuit current at reference temperature of 25^0 C and solar radiance of 1000 W/m^2= 13.1362 A

K_i = short circuit current temperature coefficient = - 0.03

Photo current at 40^0 C was obtained using equation 4.1

$$I_{ph} = \left[I_{sc} + K_i\left(T_C - T_{ref}\right)\right] \text{ x } \boldsymbol{\lambda}$$

$$I_{ph} = [13.1362 + -0.03\ (40 - 25)] \text{ x } 1$$

$$I_{ph} = [3.1362 + -0.45] = 12.6862 \text{ A}$$

The Reverse Saturation Current (Irs) of the Photovoltaic Cell

The reverse saturation current (Irs) at reference temperature and at varying temperature were obtained and the results were simulated using Matlab Simulink Software.

$$I_{rs} = I_{SC} \; / \; \left[. \exp \; \frac{(q * V_{oc})}{N_S A K T} \right] - 1$$

$$I_{rs} = \frac{13.1362}{\left[. \exp \; \frac{(1.6x\,10^{-19} * 3.1)}{82\,x\,1.13\,x\;1.38\;x\,10^{-23}\,x\,25} \right] - 1}$$

$$I_{rs} = \frac{13.1362}{[. \exp \;\; 15.5156 \;] - 1}$$

$$I_{rs} = \frac{13.1362}{5.474{,}437.0146}$$

$$I_{rs} = 2.3996\,x\,10^{-6} \text{ A}$$

The Saturation Current (Is) of the Photovoltaic Cell

The saturation current of the solar module at cell temperature of 30, 40, 60 and 80 ^{o}C were obtained as follows:

$$I_S = I_{rs\,at\,ref\,temp} \left[\frac{T_c}{T_{ref}} \right]^3 \exp \left[\frac{q\,E_G \;\; \left(\frac{1}{T_{ref}} - \frac{1}{T_c} \right)}{KA} \right]$$

$$I_S = 2.3996\,x\,10^{-6} \;\; \left[\frac{40}{25} \right]^3 \;\; \exp \left[\frac{1.6022\times10-19 \text{ X } 1.12\,eV \; \left(\frac{1}{25} - \frac{1}{40} \right)}{5.67\;\; x\,10^{-8} \;\text{X}\, 1.13} \right]$$

$$I_S = 0.0000098288 \;\; \exp\,[0.02762\,x\,10^{-15}]$$

$$I_S = 0.0000098288 \text{ A}$$

The Output Current (I) of the Photovoltaic Module

The Output Currents (I) of the Photovoltaic Module Were Determined Using Equation

$$\text{I} = I_{ph} \; - \; I_s \left[\exp \left(\frac{qV_{oc}}{AkT_c} \right) \;\; - 1 \right]$$

$$\text{I} = 12.6862 - \; 0.0000098288 \; \left[\exp \left(\frac{1.6022\times10^{-19} \;\; x\; 3.1}{1.13\;\text{X} \;\; 1.38 \;\; x\,10^{-23} \;\text{X}\, 40} \right) \;\; - 1 \right]$$

$$\text{I} = 12.6862 - \; 0.0000098288 \; [\exp(9.7106\,x\,10^{4}) \;\; - 1 \,]$$

$$\text{I} = 12.6862 - \; 0.0000098288 \; [16{,}490.493]$$

$$\text{I} = 12.6862 - \; 0.16208 = 12.5241 \text{ A}$$

T_{ref} = reference temperature

E_G = band gap energy of the semiconductor material used = 1.12 electron volt (eV)

I_{RS} = reverse saturation current at reference temperature of 25^0 C and solar radiance of 1000 W/m^2 = 2.3996 x 10^{-6} A

The Maximum Power of the Solar Module at Varying Temperature

The Maximum power of the solar module at varying temperature were obtained and presented in figure 8 and table 1. We have taken 325 W silicon solar PV module as reference in this research work. The currently highest power polycrystalline silicon 60cell module is 325W. Temperature coefficient of the maximum output power (Pmax) at STC is -0.41%/°C.

With the solar module reaching 65°C, the power loss of this module was obtained as follows; (1) 65°C – 25°C = 40°C, which is the temperature difference between the module's Pmax at STC and the temperature of 65°C reached by the cells; (2) 40°C x -0.41% = -16.4%, that means that the module loses 16.4% in power output when the cells reach 65°C; (3) Power loss in the solar module = -16.4% x 3250W = 53.3 W; (4) The maximum power this module will operate at 65°C = 271.7 W.

Table 1. Power Loss In The Solar Photo Voltaic System with Change in Temperature

S/N	Temperature	T – 25	(T -25)x -0.41	Power loss (W)	Output power (W)
1	25	0	0	0	255
2	30	5	-2.05	5.227	249.773
3	40	15	-6.15	15.683	239317
4	60	35	-14.35	36.583	218.417
5	80	55	-22.55	57.503	197.498

The Subsystem Reverse Saturation Current under Varying Temperature Conditions and the Simulink Model

The subsystem reverse saturation current takes short circuit current, electric charge, open circuit voltage, ideality factor, temperature, open circuit voltage, number of series cells and Boltzmann's constant as input parameters. The reverse saturation current (Irs) is given by

$$I_{rs} = I_{SC} / \left[. \exp \frac{(q * V_{oc})}{N_s AKT} - 1 \right]$$

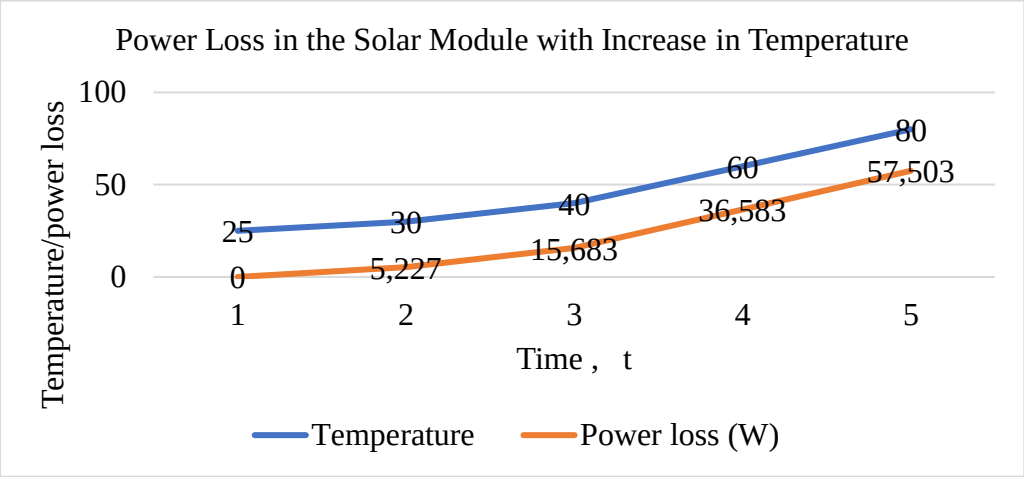

Figure 8. Power loss in the Solar Photo Voltaic System with change in temperature

Reverse saturation currents which vary with temperature were obtained and shown in table 2. The simulation results were presented in figure 9

Table 2. Irs for various temperature

S/N	Temperature (°C)	Reverse Saturation Current (A)
1	25	2.3996×10^{-6}
2	30	3.1800×10^{-5}
3	40	8.0725×10^{-4}
4	60	2.0200×10^{-2}
5	80	1.0379×10^{-1}
6	100	$2.7731 \, x \, 10^{-1}$

The Simulink model for reverse saturation current was implemented in Fig. 3.4.

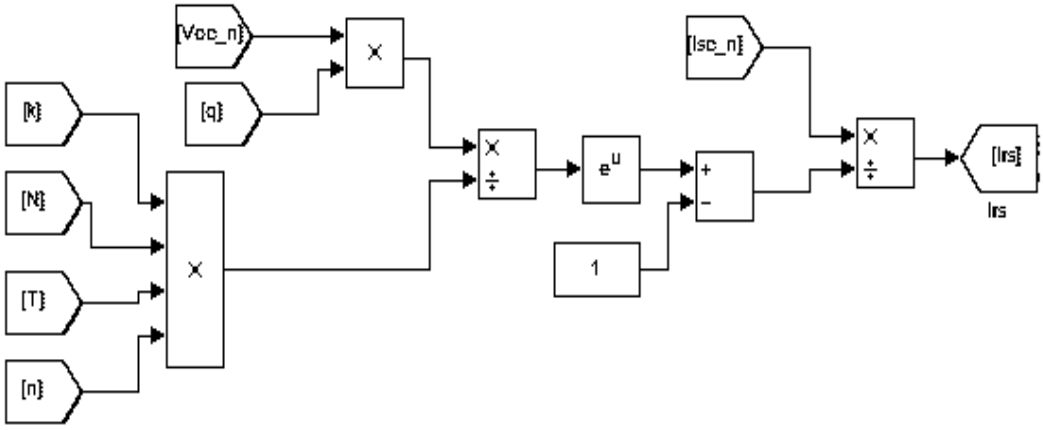

Figure 9. Subsystem of reverse saturation current

The subsystem module saturation current which varies with the cell temperature. These values were obtained and presented in table 3.

$$I_S = I_{rs} \left[\frac{T}{T_r}\right]^3 \left[\exp\left(E_{g*} \frac{q\,(T - T_r)}{A*\ K.T.T_r}\right)\right]$$

Table 3. Sauration current I_S for various temperatures

S/N	Temperature (^oC)	Saturation Current (A)
1	25	2.3996×10^{-6}
2	30	4.1465×10^{-6}
3	40	9.8280×10^{-6}
4	60	3.3172×10^{-5}
5	80	7.8600×10^{-5}
6	100	1.5357×10^{-4}

The sub-system saturation current Simulink model was implemented and the result presented in figure 10.

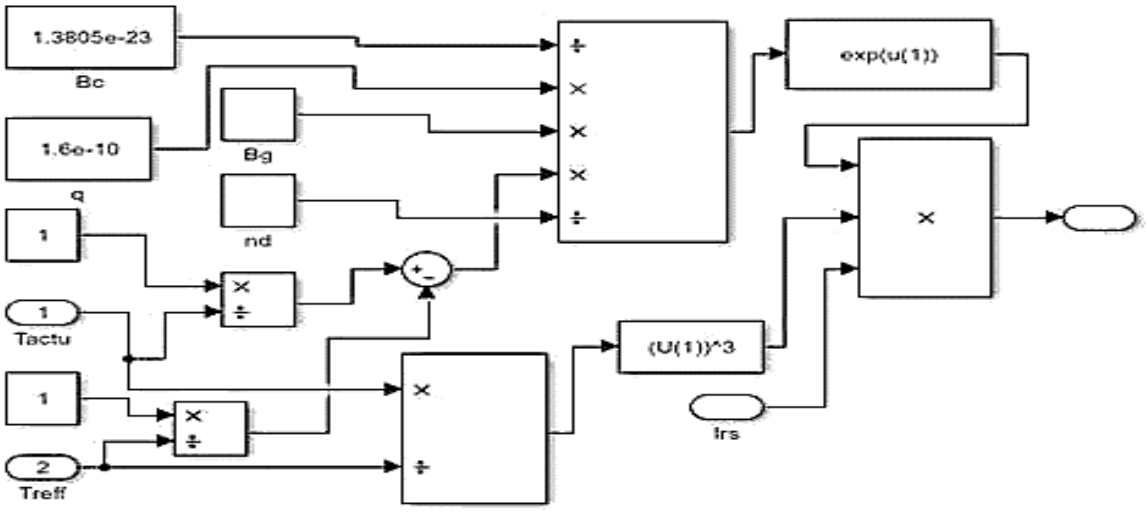

Figure 10. Subsystem of module saturation current

The Subsystem Output Current Simulink Model

The subsystem output current I_{PV} mathematical model was simulated and the result was presented in figure 11.

$$I = N_P \left[I_{ph} - I_{rs} \left\langle \exp\left(\frac{q\,(V + I\,R_S)}{AKT\,N_S} - 1\right)\right\rangle\right]$$

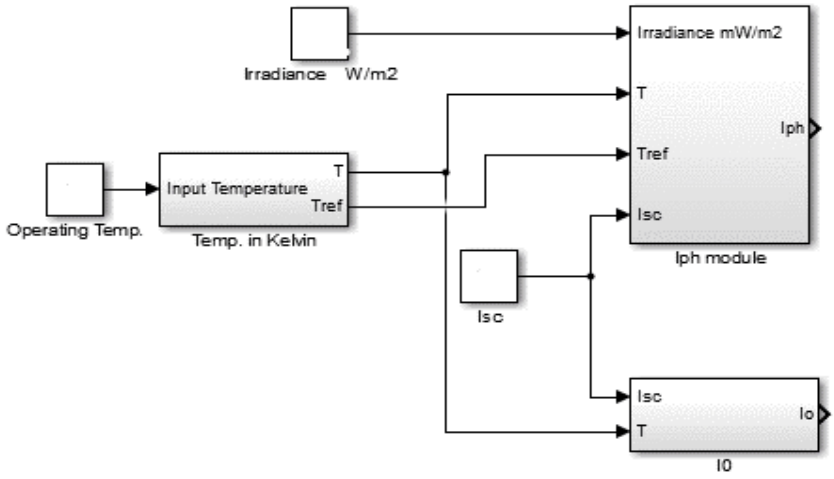

Figure 11. Subsystem of module output current.

The final model which produced the output current-voltage characteristics, and power-voltage characteristics of the solar system for varying irradiance and temperature are shown in figure 12.

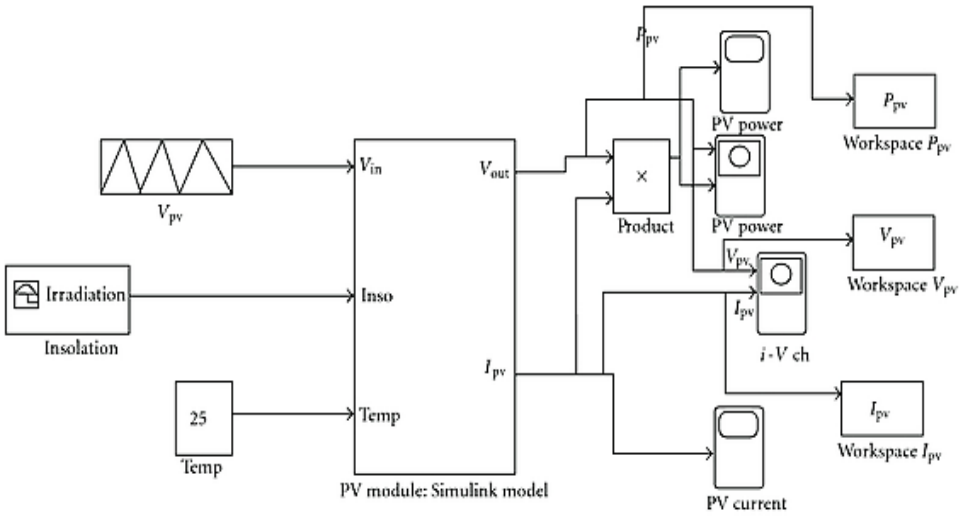

Figure 12. The final model produced the output voltage, current and power under varying irradiance and temperature

Optimum Power Point Tracking Techniques

Wind Turbine Generator Optimum Power Point Tracking Techniques

Tip Speed Ratio Control Method

Power generated in a wind turbine generator was controlled using Tip Speed Ratio (TSR) control technique. The aim of this method of optimization process was to determine the optimum TSR. From the optimum TSR, the optimum angular rotor speed was obtained.

The TSR obtained was compared with the optimum value of TSR, which is already stored in the power system. The difference in the two values of TSR is fed to the controller which adjusted angular speed of the generator in order to ensure maximum power output as shown in the figure 13.

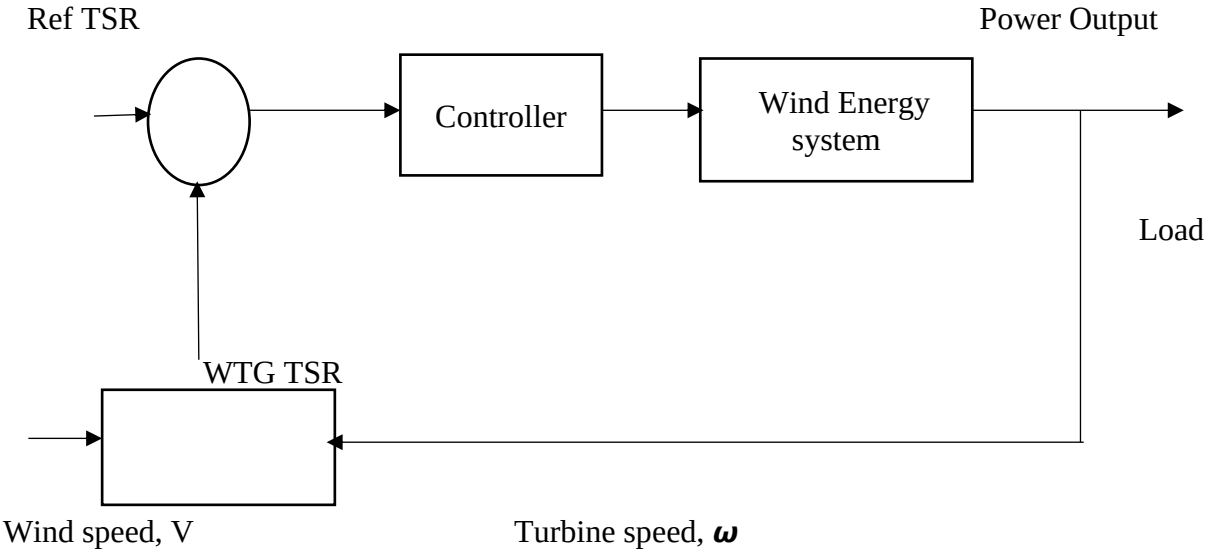

Figure 13. Working principle of TSR control techniques

Data Acquisition for the Wind Turbine Generator (WTG)

A 3.5 kW wind turbine generator proposed in Lagos State, Nigeria is taken as reference. The radius of the turbine blade is 1.12m. Average wind speed is 7m/s. Maximum Bertz coefficient of performance, C_p, is 0.5. Air density = 1.3 kg/m^3. Optimum Tip speed ratio, λ_{opt} is obtained when C_p is maximum. Optimum rotor speed, ω_{opt} is obtained during this Optimum Tip speed ratio as shown below.

Optimum Tip Speed Ratio = $\lambda_{opt} = \frac{2P}{C_p\ \rho\ A\ V^3}$

$= \frac{2\ x\ 3{,}500}{0.5\ x\ 1.3\ x\ 3.94\ x\ 7^3} = 7.9688$

The Optimum rotor speed, ω_{opt} was obtained for the proposed wind turbine generator as follows:

Optimum Rotor Speed Ratio = $\omega_{opt} = \frac{\lambda_{opt}\ x\ V}{R}$

$= \frac{7.9688\ x\ 7}{1.2} = 49.805$ rad/sec

The tip speed ratio, angular rotor speed and output power generated is presented in table 4.4a and b.

Table 4. The tip speed ratio, angular rotor speed and output power

Rω	0	33.6	36	44.8	50	56	60	67.2	75	78.4	100
Power Output (Watts)	0	1060	2100	2400	3100	3200	3100	2800	2200	1200	0

The tip speed ratio, angular rotor speed and output power generated is presented in table 4.4a

S/N	Radius of blade	ω	V	Rω	Tip Speed Ratio	Power Output
1	1.12	30	7	33.6	4.8	1,060
2	1.12	40	7	44.8	6.4	2,400
3	1.12	50	7	56.0	8.0	3,200
4	1.12	60	7	67.2	9.6	2,800
5	1.12	70	7	78.4	11.2	1,200

The tip speed ratio, angular rotor speed and output power generated is presented in table 4.4b. The characteristics of the rotor speed and the output power generated is presented in figure 14.

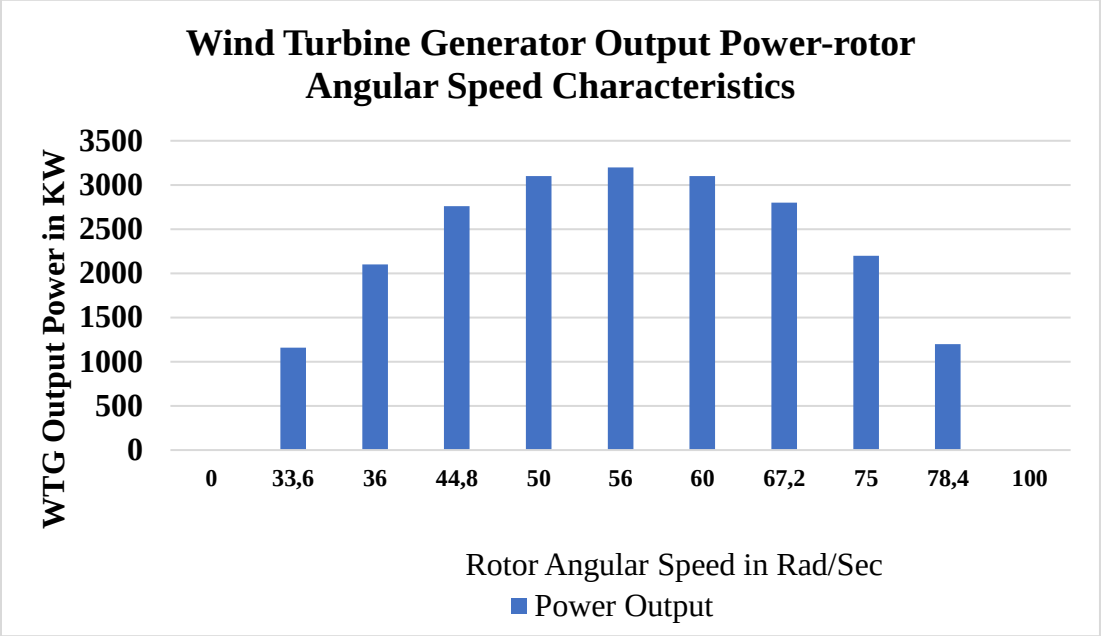

Figure 14. characteristics of the rotor speed and the output power generated from the wind turbine generator

Table 5. Shows the Monthly Output Power Produced by the Proposed Wind Turbine Generator in Watts

S/N	Months	Average Power Generated (Watts)	Average Wind Speed in m/s
1	January	1600	3.80
2	February	1800	4.22
3	March	2100	5.60
4	April	2200	5.81
5	May	2600	7.10
6	June	2100	5.60
7	July	1820	4.22
8	August	2140	5.61
9	September	3200	9.00
10	October	2860	8.40
11	November	1400	3.30
12	December	1650	4.00

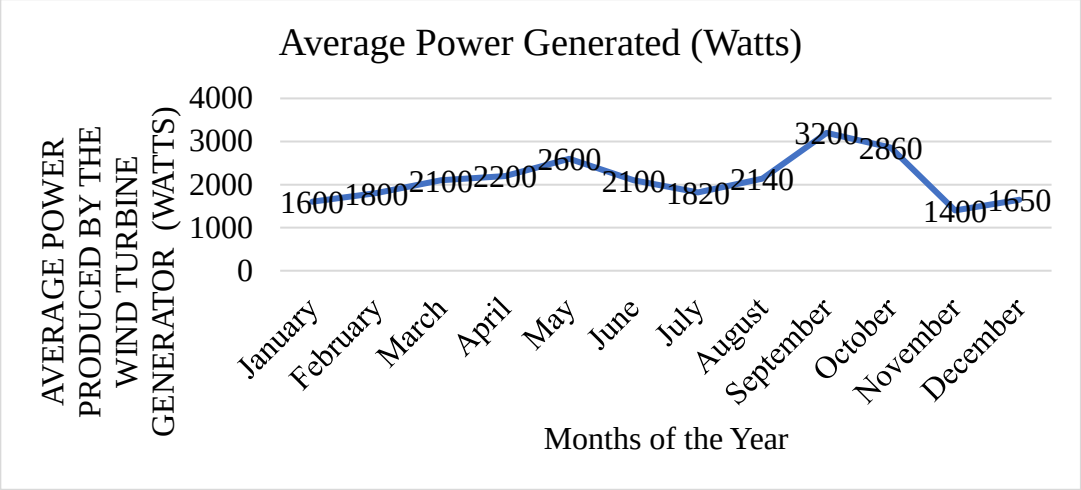

Figure 15. Monthly Output Power Produced by the Proposed Wind Turbine Generator in Watts

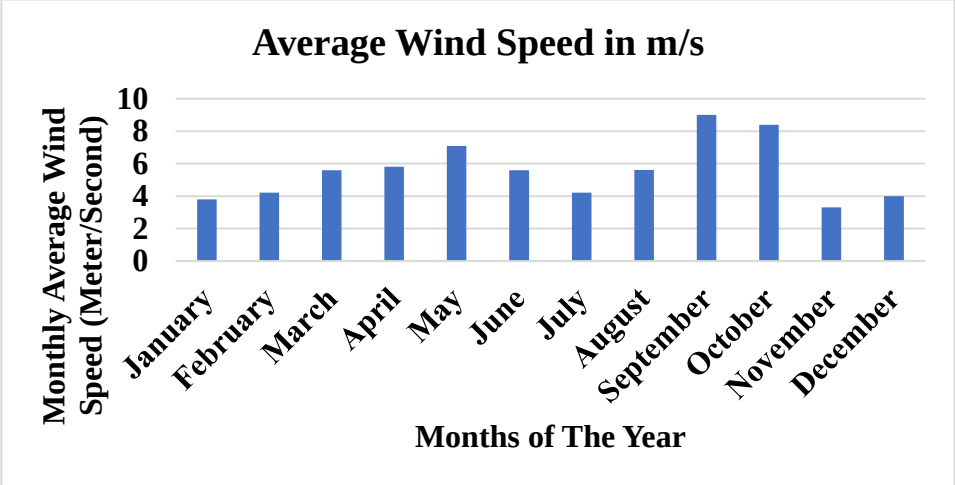

Figure 16. Monthly Average Wind Speed at the Reference Area in Meter/Second

Solar Energy Audit Data and Meteorological Data and Parameters of the Reference Site

Electrical Parameters of Photo-Voltaic cells were measured at specified temperature of 25 °C, solar irradiances 1000 W/m^2 and air mass 1.5 AM.

The number of solar panels at the reference area is 820. The solar module is 325 W each and the area of each module is 1.63m^3. The efficiency of the solar cell is 83.6 and the average annual solar radiation is 1367 kWhm^{-2}.

Energy consumption at the study area in watt hour = 1,865,500 Watt hour

This implies that the total energy to be supplied = 1,865,500 Wh

$$\text{Watt peak} = \frac{\text{Energy to be supplied}}{number\ of\ hours\ of\ sunlight}$$

$$\text{Watt peak} = \frac{1{,}865{,}500\ \text{Wh}}{7} = 266{,}500$$

$$\text{Number of 325 W panels} = \frac{\text{Watt peak}}{Wattage\ of\ a\ solar\ panel}$$

$$\text{Number of 325 W panels} = \frac{266{,}500}{325} = 820$$

System voltage = Voltage of a battery x number of batteries in series

= 12 X 10 = 120 V

Charge to be stored in the solar system = $\frac{Grand\ total\ energy\ x\ Day(s)\ of\ autonomy}{System\ Voltage}$

Charge to be stored in the solar system = $\frac{1{,}865{,}500\ x\ 1}{120}$

= 15,545.833 Ampere hour (Ah)

System Current = $\frac{\text{Total power}}{system\ voltage}$ = $\frac{245{,}073.4}{120}$ = 510.57 A

200 Ah batteries were proposed at the reference area

Number of batteries required = $\frac{\text{Charge to be stored in the solar system}}{rating\ of\ a\ battery\ in\ Ah\ x\ depth\ of\ discharge}$

Hence, number of batteries required = $\frac{15{,}545.833}{200\ x\ 0.2}$ = 388.65 = 387

Average solar insolation: 278–330 days of sun per year with daily average sunshine ranging from7 hours during the rainy season to 9 hours in dry season.

Solar radiation: 833.33 to 1341.67 kWh/m^2

Subsystem of photon generated current Iph for different values of irradiance and temperature were presented in table 6.

Table 6. Subsystem of Photo Generated Current under varying temperature and irradiance

S/N	Temperature (°C)	Irradiance kW/m^2	Photo current (A)
1	25	1	13.1362
2	30	1	12.986
3	40	1	12.6862
4	60	1	12.0862
5	80	1	11.4862
6	100	1	10.8865

$$I_{ph} = I_{SCR} + k_1 [T - T_r] \frac{S}{100}$$

$$I_{ph} = I_{SCR} + k_1 [T - T_r] \lambda$$

The subsystem reverse saturation current takes short circuit current, temperature, open circuit voltage, number of series cells as input parameters. The reverse saturation current (Irs) is given b

$$I_{rs} = I_{SC} / \left[. \exp \frac{(q * V_{oc})}{N_S AKT} - 1 \right]$$

Reverse saturation currents vary with temperature were obtained and shown in table 7

Table 7. reverse saturation current Irs for various temperature

S/N	Temperature (°C)	Reverse Saturation Current (A)
1	25	2.3996×10^{-6}
2	30	3.1800×10^{-5}
3	40	8.0725×10^{-4}
4	60	2.0200×10^{-2}
5	80	1.0379×10^{-1}
6	100	$2.7731x\ 10^{-1}$

The subsystem of module saturation current which varies with the cell temperature were obtained and presented in table 7.

$$I_S = I_{rs} \left[\frac{T}{T_r}\right]^3 \left[\exp\left(E_{g*} \frac{q\,(T - T_r)}{A*\ K.T.T_r}\right)\right]$$

Table 8. Sauration current I_S for various temperatures

S/N	Temperature (^oC)	Saturation Current (A)
1	25	2.3996×10^{-6}
2	30	4.1465×10^{-6}
3	40	9.8280×10^{-6}
4	60	3.3172×10^{-5}
5	80	7.8600×10^{-5}
6	100	1.5357×10^{-4}

Simulation Results

The constructed model was applied to the module example, and the outcomes were assessed. Utilizing the previously derived equations, the assessment was conducted. The selected module produces 255W of output power and consists of 10 series cells. The IV and PV characteristics are modeled and simulated for the chosen module using the developed equations and models. Figure 17 and figure 18 show the IV and PV characteristics of module under varying irradiance at constant temperature respectively.

Table 9. I-V Curves with various Irradiance levels

I - V Curves	**Temperature in Kelvin 273 + T ref**	**Irradiance level in KW/m^2**
A	298	1
B	298	0.8
C	298	0.6
D	298	0.4

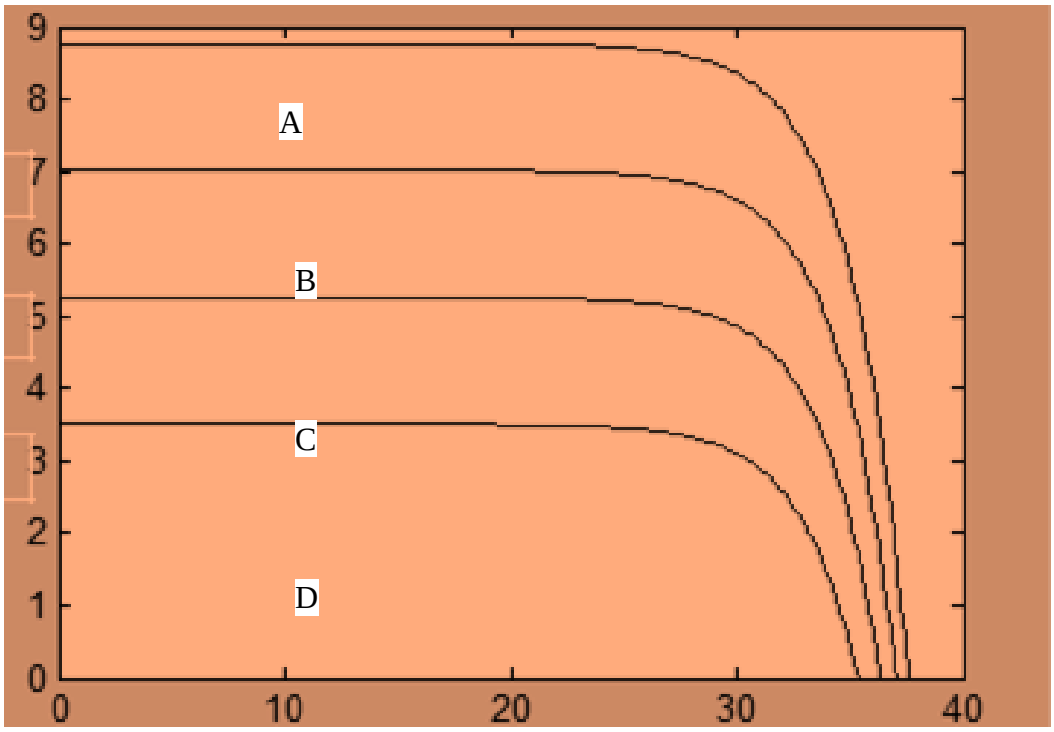

Figure 17. IV characteristics under varying irradiance at constant temperature (298K)

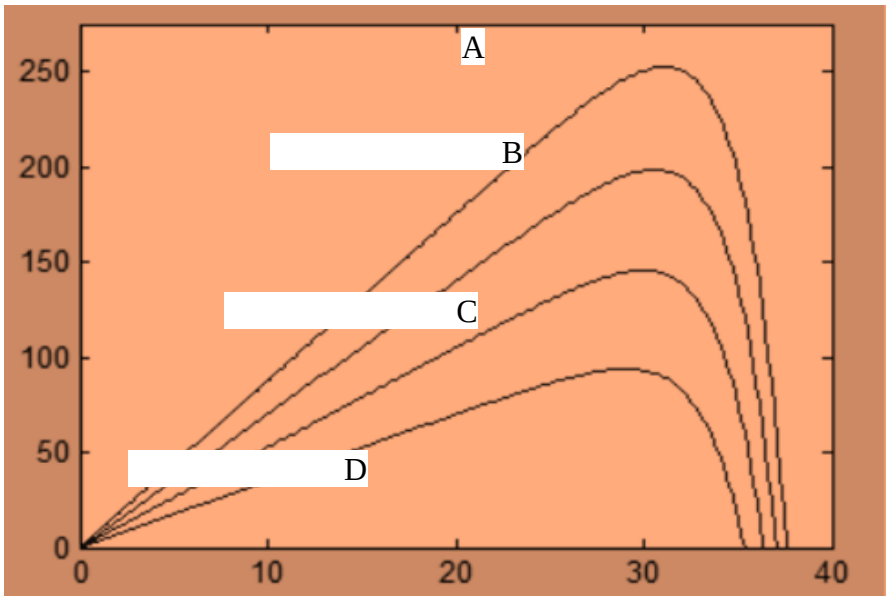

Figure 18. PV characteristics under varying irradiance at constant temperature (298K)

Figures 17 and 18 show the module's IV and PV properties at various temperatures and constant irradiation, respectively. According to the features, there is an optimal operating point known as maximum power point. This point varies as a function of temperature and irradiance. This point rises with increasing irradiance and falls with increasing temperature. Thus, it was able to predict the optimal power point for the solar system in question.

Table 10. I-V Curves with various temperature levels

I – V Curves	Irradiance level in KW/m^2	Temperature in Kelvin
A	1	298
B	1	318
C	1	338
D	1	358

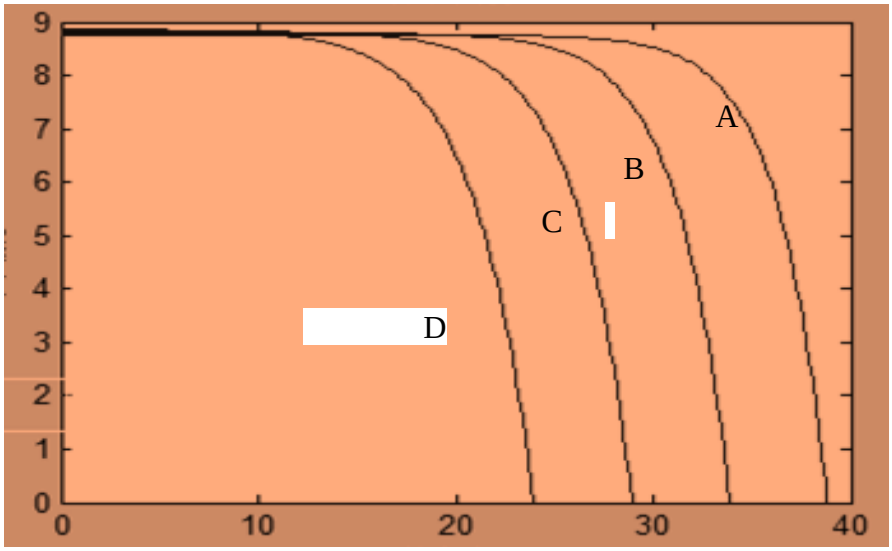

Figure 19. IV characteristics under varying temperature at constant irradiance (1KW/m^2)

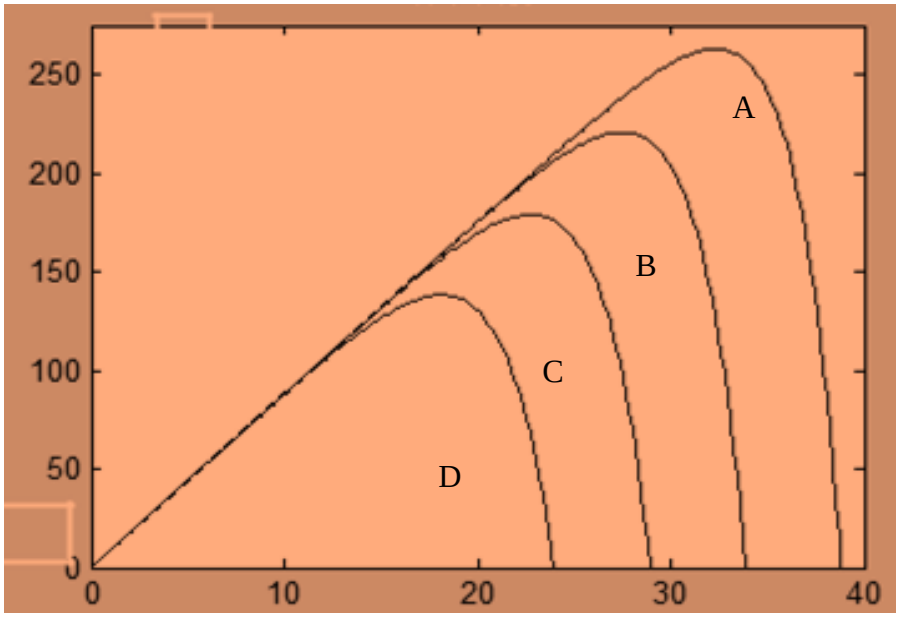

Figure 20. PV characteristics under varying temperature at constant irradiance (1KW/m^2)

Matlab/Simulink was used to create and simulate a photovoltaic (PV) module. According to the model, the output current is a function of solar irradiation. The created PV model is validated using a module that is currently accessible. The model might be used for solar photovoltaic conversion system and MPPT technology examination.

Table 12. shows the Average monthly radiation of the reference area in kWh/meter square

S/N	Months	Average monthly radiation (kWh/meter square)
1	January	6.86
2	February	6.58
3	March	6.72
4	April	4.34
5	May	4.06
6	June	3.64
7	July	3.22
8	August	5.01
9	September	3.78
10	October	5.74
11	November	6.3
12	December	6.44

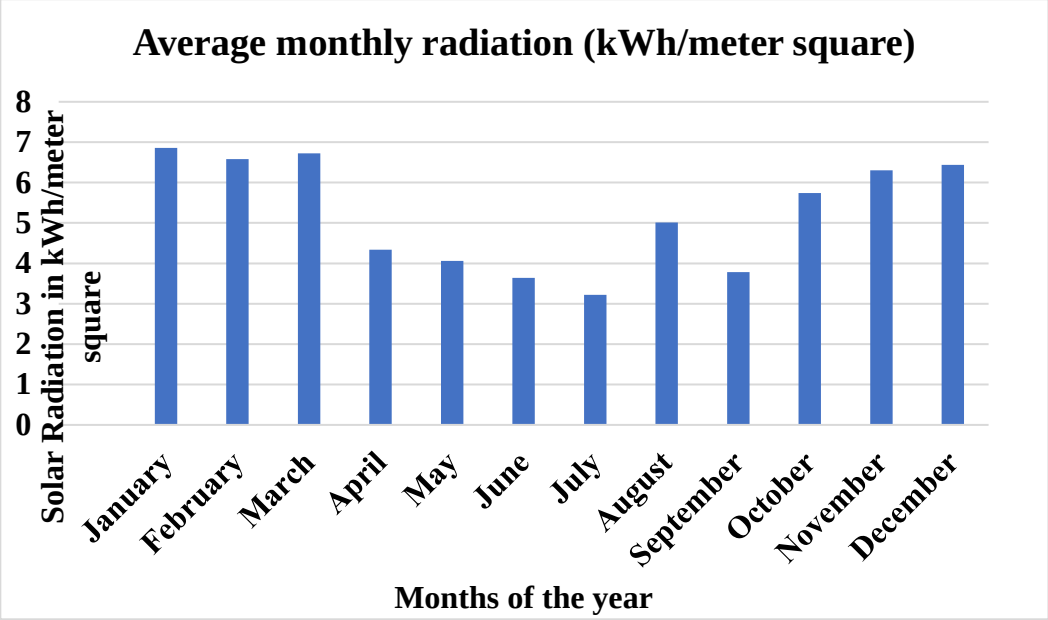

Figure 21. shows the Average monthly radiation of the reference area in kWh/meter squar

Conclusion

Solar Radiation and Power Generation from the Solar Photo-Voltaic System

Annual solar radiation at the reference area ranges between 3.22 kwh/m^3 to 6.86 kwh/m^3. the value of sun radiation in the study area is very high in the month of october – march i.e., during the dry season. the study revealed that the solar radiation during this period ranges between 5.74 kwh/m^3 to 6.86 kwh/m^3. hence, the hybrid electric power system (heps) developed produced adequate and reliable solar electric power system between the six months as shown in tables 4.13 – 4.21 and figures 4.12, 4.14, 4.17 – 4.23. the reliability of the solar photo-voltaic power system during this period is 100%. the photo-current and reverse saturation current were presented in tables 4.5 and 4.6 respectively.

However, solar radiation reduces during the months of april – september to the range of 3.22 kwh/m^3 to 4.34 kwh/m^3 as shown in figure 4.11. consequently, the solar power generated during the rainy season reduces to 154w – 174w/module as presented in figure 4.16. weather condition during this period reduced solar radiation and the electric power generated from the solar photo- voltaic system (spvs). as a result, the efficiency and relisability of the system reduces considerably. therefore, the provision of other reliable power supply system increased the reliability of the system and ensured continuous supply of electrical energy to the consumers.

Solar Photo- Voltaic System (Spvs) and Hydro Electric Power System (Heps)

Through the building of a recommended hydroelectric power plant, this research has presented a suitable solution to the problem of solar photovoltaic systems' unreliability. As shown in tables 4.3 and 4.4, the projected power plant's production capacity during the wet season varies from 4,948.88 kw to 6,245.01 kw. The discharge rate of the Ikere River in the iseyin village of Oyo State, where the proposed hydroelectric power plant would be located, ranges from 13.8 m (3)/second in February to 31.8 m(3)/second in September. Table 4.4 and images 4.2, 4.3, 4.13, 4.20, 4.22, and 4.23 correspondingly exhibit this information. During this time period, the generated output power varied between 4,948,88 kw and 6,245,01 kw. As a direct result, it became possible to offer clients with sufficient and continuous power supply.

Solar Photo-Voltaic System Simulation Results

The simulation results presented in figures 4.4 – 4.7 show that solar power generated from the solar modules increases with increase in radiation and reduces as temperature rises above $25^0 c$. table 4.10 represents variation of power loss in the photo-voltaic system with change in temperature. figures 4.12 – 4.18 show the monthly electric power production from the hybrid solar photo-voltaic system, proposed hydro-electric power plant, proposed wind turbine generator and the diesel generator. the hybrid-electric power system produced adequate, reliable, stable power supply as shown in figures 4.19 - 4.23.

Reference

Aliyu, A. S., Dada, J. O., & Adam, I. K. (2015). Current status and future prospects of renewable energy in Nigeria. *Renewable and sustainable energy reviews*, *48*, 336-346.

Austin, O. O. (2021). Advanced Control And Development of Hydro and Diesel Generator Hybrid Power System Models for Renewable Energy Microgrids. *Journal La Multiapp*, *2*(3), 16-32. https://doi.org/10.37899/journallamultiapp.v2i3.383**.**

Austin, O. O., Alonge, O., & Adeniyi, A. J. (2020). Fault Diagnosis Algorithm and Protection of Electric Power Systems in an Alternative Distribution System. International *Journal* of Advanced Trends in Computer Science and Engineering, pp 8-16. https://doi.org/10.37899/journallamultiapp.v1i3.192.

Austin, O. O., Lasisi, K. A., Adeniyi, A. J., & Alonge, O. (2020). Development of a Model for the Establishment of a Hydro Electric Power Generating Plant. *Journal La Multiapp*, *1*(3), 27-42. https://doi.org/10.37899/journallamultiapp.v1i3.207.

Bekele, G., & Tadesse, G. (2012). Feasibility study of small Hydro/PV/Wind hybrid system for off-grid rural electrification in Ethiopia. *Applied Energy*, *97*, 5-15.

Bhandari, B., Poudel, S. R., Lee, K. T., & Ahn, S. H. (2014). Mathematical modeling of hybrid renewable energy system: A review on small hydro-solar-wind power generation. *international journal of precision engineering and manufacturing-green technology*, *1*(2), 157-173.

Engin, M. (2013). Sizing and simulation of PV-wind hybrid power system. *International journal of photoenergy*, *2013*.

Fadaeenejad, M., Radzi, M. A. M., AbKadir, M. Z. A., & Hizam, H. (2014). Assessment of hybrid renewable power sources for rural electrification in Malaysia. *Renewable and Sustainable Energy Reviews*, *30*, 299-305.

Hua, C., & Lin, J. (2004). A modified tracking algorithm for maximum power tracking of solar array. *Energy Conversion and Management*, *45*(6), 911-925.

Iqbal, M. M., & Islam, K. (2017). Design and simulation of a PV System with battery storage using bidirectional DC-DC converter using Matlab Simulink. *International Journal of scientific & Technology research*, *6*(07), 403-410.

Jain, M., & Ramteke, N. (2013). Modeling and simulation of solar photovoltaic module using matlab/simulink. *Journal of Computer Engineering*, *15*(5), 27-34.

Kumar, N. M., Chopra, S. S., Chand, A. A., Elavarasan, R. M., & Shafiullah, G. M. (2020). Hybrid renewable energy microgrid for a residential community: A techno-economic and environmental perspective in the context of the SDG7. *Sustainability*, *12*(10), 3944.

Kyari, I. B., & Muhammad, J. Y. U. (2019). Hybrid Renewable Energy Systems for Electrification: A Review. *Science Journal of Circuits, Systems and Signal Processing*, *8*(2), 32.

Nwaigwe, K. N., Mutabilwa, P., & Dintwa, E. (2019). An overview of solar power (PV systems) integration into electricity grids. *Materials Science for Energy Technologies*, *2*(3), 629-633.

Nwokoye, E. S., Dimnwobi, S. K., Ekesiobi, C. S., & Obegolu, C. C. (2017). Power infrastructure and electricity in Nigeria: Policy considerations for economic welfare. *KIU Journal of Humanities*, *2*(1), 5-17.

Salilih, E. M., & Birhane, Y. T. (2019). Modeling and analysis of photo-voltaic solar panel under constant electric load. *Journal of Renewable Energy*, *2019*.